SIMULATIONS OF THE WATER FREEZING PROCESS – NUMERICAL BENCHMARKS

TOMASZ MICHAŁEK AND TOMASZ A. KOWALEWSKI

Institute of Fundamental Technological Research,
Polish Academy of Sciences,
Department of Mechanics and Physics of Fluids,
Świętokrzyska 21, 00-950 Warsaw, Poland
tmichal@ippt.gov.pl

Abstract: Three numerical benchmarks concerning the freezing of water in small enclosures are analysed using the commercial FLUENT code. The first case is a steady-state natural convection in a differentially heated cavity for temperatures near the freezing point. In the second case, the freezing of water in a differentially heated cavity is simulated. The third case describes a simulation of freezing water in the presence of forced convection and a free surface flow. Two finite-differences numerical codes are used to verify results of the FLUENT simulations for the natural convection and solidification in the differentially heated cavity. It is found that the simulation of water solidification requires very fine meshes and short time steps, extending the computational time to the extreme.

Keywords: numerical simulation, numerical benchmarks, finite volume method, fixed grid enthalpy-porosity method, volume of fluid, solidification, free surface flow

1. Introduction

The simulation of solidification processes is still a challenging task for numerical modelling. Such modelling became to play an important role in several branches of industry, including the foundry industry (in continuous casting of metals), welding, the material industry (in composite materials and crystal growth), cryosurgery and food conservation. Solidification is also present in several natural processes, like iceberg evolution, magma chambers or crust formation. Direct application of numerical methods to the engineering or environmental problems is not a trivial task. It is due to the usual complexity of geometry, variable and often not exactly known thermal properties of both phases, a moving interface, non-linearity of the underlying equations and difficulties in precise estimation of thermal and initial boundary conditions [1, 2]. Hence, in the recent years, special attention has been paid to the formulation of numerical and experimental benchmarks based on simple geometry and fluids of well-known properties [3, 4]. Such experimental and numerical benchmarks are useful for establishing a proper physical model or for verifying new numerical methodologies.

They can be applied for tuning and validating numerical codes before they are applied to industrial tasks.

The aim of this work is to apply the finite volume code FLUENT 6.0 (Fluent Inc. [5]) to define three benchmark solutions for water freezing in small rectangular containers. It is generally recognised that the phase change processes are mostly influenced by natural convection. Additionally there is a close relationship between the convective flow in the melt and the structure of the solid formed in the solidification process [6]. Hence, the first benchmark concerns modelling of steady-state natural convection of water in a differentially heated cavity. Although this numerical model does not contain solidification, an anomaly of water density variation close to the freezing point creates an interesting and challenging numerical problem. The steady-state flow pattern established during the pure convection phase decides about the later development of the solidification front. Hence, the first benchmark solution is used as an initial condition for the second benchmark – modelling of water freezing in a differentially heated cavity. The last benchmark concerns modelling of solidification in the presence of a free surface flow. In this case, flow is driven not only by natural convection, but also by forced convection. We believe that this benchmark can be useful for verifying numerical codes used for modelling casting problems, where the interior of a complex geometry is filled during the solidification process.

The finite volume solver of FLUENT uses an enthalpy-porosity fixed-grid method for modelling the phase change [7] and the volume of fluid (VOF) method to model the free surface flow. We performed 2D and 3D calculations assuming incompressible laminar viscous flow. The anomalous water density variation was implemented in the buoyancy term. All remaining material properties of water and ice, like thermal conductivity, viscosity and specific heat, were assumed to be constant.

The numerical results obtained with FLUENT for the first two problems, *i.e.* natural convection and freezing in differentially heated cavity, were compared with two reference codes: FRECON3V [8] and NC4MARV2 [9]. FRECON3V is a revised, three-dimensional, variable properties version of FRECON [10].

In the following, we give a brief description of the numerical model used for the three investigated configurations, details of material properties and discrete schemes, boundary and initial conditions, followed by examples of results and their discussion.

2. Natural convection of water in a differentially heated cavity

2.1. Problem formulation

We consider natural convection of water in the differentially heated cubic cavity of a height L. Two vertical walls are isothermal, kept at temperatures T_H, T_C. All remaining walls are assumed to be adiabatic. The temperature difference between the vertical walls $\Delta T = T_H - T_C$ is 10K. The initial temperature of the fluid is set at $T_0 = 278$K. Both two and three-dimensional simulations have been performed, but for the sake of brevity we have given below only the mathematical formulation for the two-dimensional case.
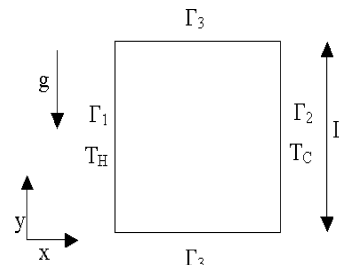
2.2. Mathematical formulation

The basic equations modelling natural convection describe conservation of mass, momentum and energy:

$$\frac{\partial u}{\partial x} + \frac{\partial w}{\partial y} = 0, \tag{1}$$

$$\rho_0 \frac{\partial u}{\partial t} + \rho_0 u \frac{\partial u}{\partial x} + \rho_0 w \frac{\partial u}{\partial y} = -\frac{\partial p}{\partial x} + \mu \Delta u, \tag{2}$$

$$\rho_0 \frac{\partial w}{\partial t} + \rho_0 u \frac{\partial w}{\partial x} + \rho_0 w \frac{\partial w}{\partial y} = -\frac{\partial p}{\partial y} + \mu \Delta w - g[\rho(T) - \rho_0], \tag{3}$$

$$\frac{\partial T}{\partial t} + u \frac{\partial T}{\partial x} + w \frac{\partial T}{\partial y} = \alpha \Delta T. \tag{4}$$

The above equations describe two-dimensional flow of an incompressible viscous fluid, where u, w, ρ_0, p, μ, g, T, α denote horizontal and vertical velocities, the reference density of the fluid, pressure, dynamic viscosity, gravitational acceleration, temperature and thermal diffusivity, respectively. Water properties, like dynamic viscosity, specific heat, thermal conductivity and density are assumed to be constant. The anomalous thermal variation of water density is implemented in the buoyancy term only (Equation (3)). The fourth order polynomial $\rho(T)$ given by Kowalewski and Rebow [3] is used here. Material properties used in the numerical model are provided in Table 1. Thermal boundary conditions for isothermal walls have been taken as $T|_{\Gamma_1} = T_H = 283\mathrm{K}$ and $T|_{\Gamma_2} = T_C = 273\mathrm{K}$; for adiabatic walls $\frac{\partial T}{\partial n}|_{\Gamma_3} = 0$. Standard no-slip boundary conditions at the walls have been adopted for the velocity components. The initial conditions are $T(0) = T_0 = 278\mathrm{K}$ for temperature and $\vec{v}_0 = (u, w) = 0$ for the velocity field. Dimension of the cavity L is 38mm.

Table 1. Properties of water used in the simulations

	Material properties of water	Value	Unit
ρ_0	density of water at reference temperature $T_{ref} = 273\mathrm{K}$	999.8	kg/m^3
μ	dynamic viscosity (at $T = 288\mathrm{K}$)	0.001003	kg/ms
$\nu = \mu/\rho_0$	kinematic viscosity (at $T = 288\mathrm{K}$)	$1.0032 \cdot 10^{-6}$	m^2/s
κ	thermal conductivity (at $T = 288\mathrm{K}$)	0.6	W/mK
c_p	specific heat (at $T = 288\mathrm{K}$)	4182.0	J/kgK
g	gravitational acceleration	9.81	m/s^2
$\alpha = \kappa/(\rho_0 c_p)$	thermal diffusivity (at $T = 288\mathrm{K}$)	$1.435 \cdot 10^{-7}$	m^{2}s
β_0	thermal expansion coefficient (at $T = 273\mathrm{K}$)	$6.734 \cdot 10^{-5}$	1/K

The dimensionless parameters defining the problem are the Rayleigh and Prandtl numbers: $\mathrm{Ra} = g\beta_0(T_H - T_C)L^3/\alpha\nu = 2\,518\,084$, $\mathrm{Pr} = \nu/\alpha = 6.99$. Dimensionless variables for temperature ϑ, horizontal and vertical coordinates $\tilde{x}$, $\tilde{y}$, horizontal and vertical velocities $\tilde{u}$, $\tilde{w}$, and time $\tilde{t}$, have been defined as follows: $\vartheta = (T - T_C)/(T_H - T_C)$, $\tilde{x} = x/L$, $\tilde{y} = y/L$, $\tilde{u} = uL/\alpha$, $\tilde{w} = wL/\alpha$, $\tilde{t} = t\alpha/L^2$.

2.3. Numerical algorithms and mesh sensitivity test

Steady-state two- and three-dimensional solutions for the problem defined above were obtained using the finite volume code FLUENT 6.0 on uniform structural

grids (details are given it Table 2). The implicit false transient method was used to reach efficiently a steady-state. Spatial derivatives were approximated using the QUICK scheme, which is based on a weighted average of second-order-upwind and central interpolation of the variable. Pressure-velocity coupling was done with the SIMPLE algorithm, introduced by Patankar [11]. For comparison the same problem was solved using the FRECON3V finite difference code [4], which is based on the vorticity-vector potential formulation of the Navier-Stokes and energy equations for laminar flow of a viscous, incompressible fluid. As FRECON3V is essentially a 3D code, two-dimensional solutions were simulated using 5 grid points in depth and no-slip, adiabatic conditions for the side walls in the third dimension.

Table 2. Discretization meshes used in the calculation

Run No	Mesh name/code	Size	Number of nodes	Number of elements
#1	2d0005/FLUENT	76×76	5 929	5 776
#2	2d0002/FLUENT	190×190	36 481	36 100
#3	2d0001/FLUENT	380×380	145 161	144 400
#4	3d0005/FLUENT	$76 \times 76 \times 76$	456 533	438 976
#5	3d0002/FLUENT	$190 \times 190 \times 190$	6 867 871	6 859 000
#6	2df81×81/FRECON3V	81×81	6 724	6 561
#7	3df81×81×81/FRECON3V	$81 \times 81 \times 81$	551 368	531 441

The mesh sensitivity analysis performed for FLUENT (Table 2) shows that two-dimensional solutions converge for both refined meshes (run #2 and #3). We may estimate that a local error of the velocity and temperature results obtained for run #3 is below 3%. Figure 1 shows temperature and velocity profiles along the horizontal and vertical symmetry lines of the cavity for meshes from Table 2. It is worth noting that the errors of simulation performed for the quite fine mesh (run #1) may reach almost 50% for vertical velocity (compare Figure 1f). Large errors also occur for the horizontal velocity component obtained for the coarse mesh (Figure 1d). This test indicates that modelling a simple natural convection in the presence of strongly non-linear variation of water density requires careful analysis of results and very fine meshes.

2.4. Analysis of numerical results

Results for temperature, velocity and stream-function fields obtained for the most accurate run #3 are presented in Figures 2a and 2c. Due to anomalous thermal variation of water density, the flow structure consists of two competing circulations, easily discernible in the velocity field and the stream-function contour (Figures 2b and 2c). In the vicinity of the cold wall, normal and abnormal convection streams collide forming a clearly visible saddle point. These two-dimensional results seem to be in good agreement with the three-dimensional simulation (run #5) displayed for the central cross-section of the cavity (Figure 2d). Then, the two-dimensional FLUENT simulation (run #3) is compared with the reference solution obtained using the FRECON3V numerical code (run #6). A detailed comparison of the velocity and temperature profiles is given in Figure 3. It can be found that, despite a relatively

(a)

(b)

(c)

(d)

(e)

(f)
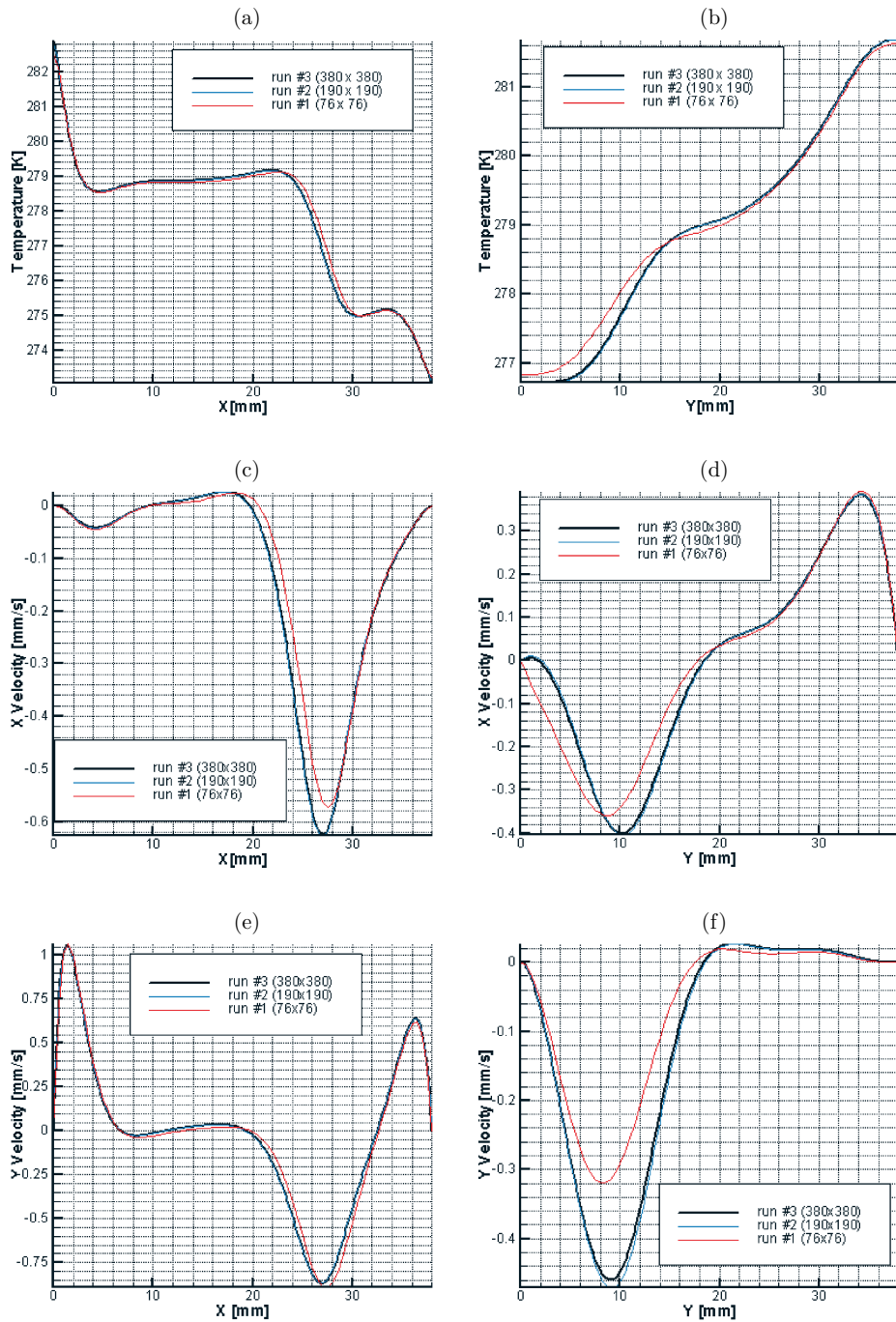
Figure 1. Mesh sensitivity test of two-dimensional simulations obtained with FLUENT (runs #1, #2, #3); profiles of temperature (top), the horizontal velocity component (middle) and the vertical velocity component (bottom), obtained along the horizontal symmetry lines (left column) and the vertical symmetry line (right column) of the cavity

(a)

(b)

(c)

(d)
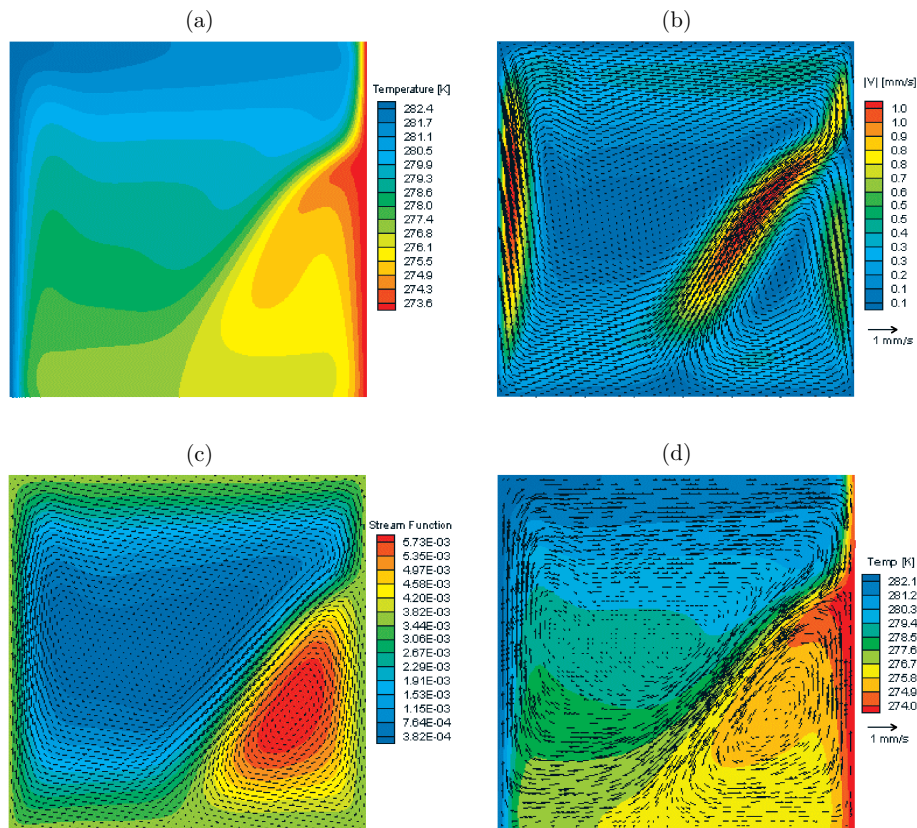
Figure 2. (a) Contours of temperature (run #3); (b) velocity field and velocity magnitude contour (run #3); (c) velocity field and stream function contours (run #3); (d) velocity field and temperature contours (run #5)

coarse mesh, results obtained with the FRECON3V university code are very close to those of the costly FLUENT solution. Both temperature and velocity profiles practically overlap, and local discrepancies are below 3%.

Two- and three-dimensional simulations performed with both of the analysed codes are compared along the vertical line passing through the velocity saddle point ($x = 0.93$). As can be seen in Figure 4b, two-dimensional and three-dimensional results obtained with FRECON3V are practically identical and overlap with the three-dimensional solution obtained with FLUENT. However, the two-dimensional solution obtained with FLUENT (run #3) shows slight deviations. It is a rather surprising result, requiring more detailed analysis of two and three-dimensional solvers applied in FLUENT.

3. Water freezing in a differentially heated cavity

3.1. Problem formulation

The second problem concerns the modelling of water freezing in a differentially heated cavity. The computational domain is the same cube-shaped cavity as in the previous case. We consider freezing of water after the thermal boundary condition is
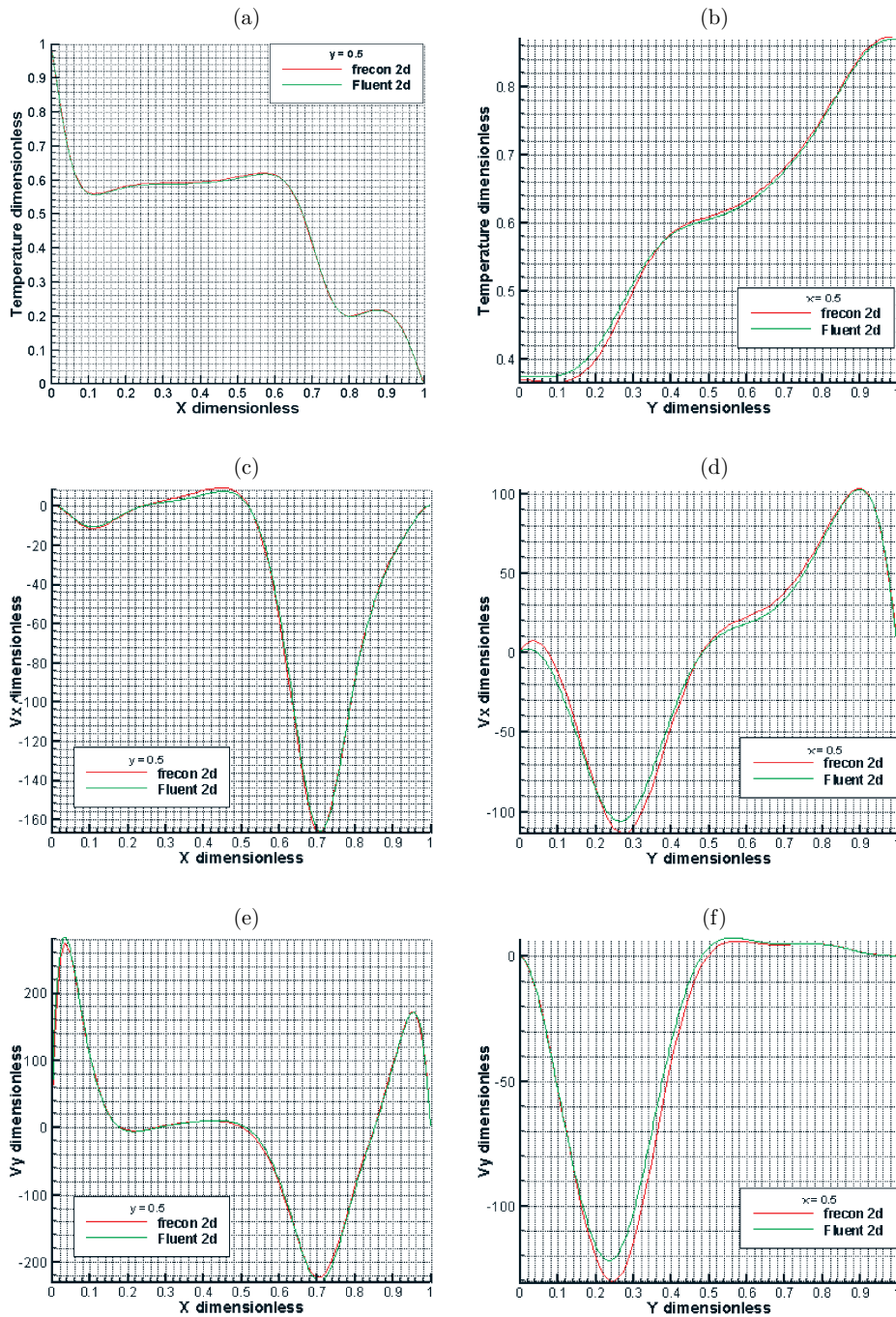
Figure 3. Comparison of two-dimensional simulations obtained with FLUENT (run #3) and FRECON3V (run #6). Profiles of temperature (top), horizontal velocity component (middle), and vertical velocity component (bottom) obtained along the horizontal (left column) and vertical (right column) symmetry lines of the cavity

(a)
(b)
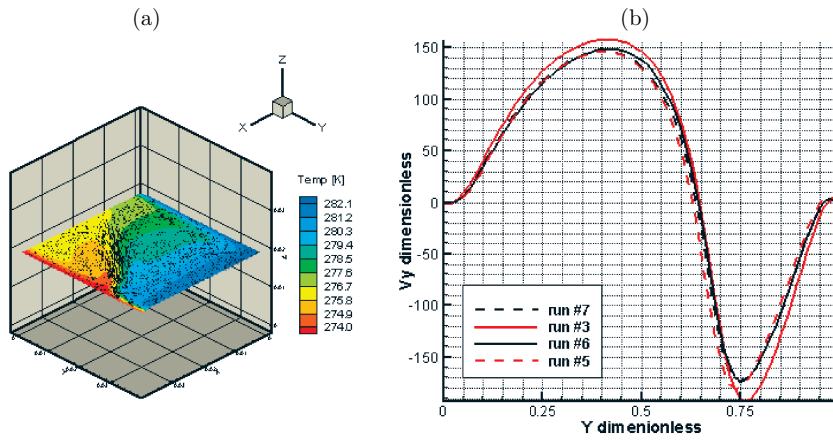
Figure 4. (a) Velocity vectors and temperature field in the central cross-section of the cavity ($Z = 0.5$) for run #5; (b) Comparison of 2D and 3D simulations with FLUENT (runs #3, #5) and FRECON3V (runs #6, #7); profiles of the vertical velocity component at the central cross-section along line $x = 0.93$

abruptly changed from $T_c = 273\mathrm{K}$ to $T_c = 263\mathrm{K}$ at the cold wall. The steady-state convection pattern obtained in the previous case becomes the initial condition for the temperature and velocity fields in the fluid domain. A FLUENT solver is used to obtain two-dimensional transient solutions describing the development of velocity and temperature fields as the solidification front propagates from the cold wall. The NC4MARV2 2D finite volume university code is used for comparison.

3.2. Mathematical formulation

A fixed grid-enthalpy method is used in both codes to simulate the freezing process [7]. This method uses a single set of conservation equations and boundary conditions for the whole domain. The interface conditions between the solid and the liquid phase are accounted for by incorporating a suitable source term in the governing equations. Total heat content (enthalpy) and the liquid fraction function have to be defined to present a unique set of equations.

Liquid fraction is a function of temperature, varies from 0 to 1 and defines volumetric ratio of the liquid phase in a computational cell:

$$f_l = \begin{cases} 0 & \text{if } T < T_s \\ \frac{T - T_s}{T_l - T_s} & \text{if } T_s < T < T_l \\ 1 & \text{if } T_l < T \end{cases} \tag{5}$$

Using the definition of liquid fraction, f_l, the total heat content for a fluid (or the enthalpy function), $h(T)$, can be defined as:

$$h(T) = \int_{T_{ref}}^{T} c_p dT + f_l \lambda. \tag{6}$$

Here, λ denotes latent heat required for a phase change, and T_l, T_s denote the liquidus and solidus temperatures for the fluid.

The governing equations can be written in the following way:

$$\rho_0 \left[\frac{\partial}{\partial t}(c_p T) + u\frac{\partial}{\partial x}(c_p T) + w\frac{\partial}{\partial y}(c_p T) \right] = \kappa \Delta T - \rho_0 \lambda \frac{\partial f_l}{\partial t}, \tag{7}$$

$$\frac{\partial u}{\partial x} + \frac{\partial w}{\partial y} = 0, \tag{8}$$

$$\rho_0 \frac{\partial u}{\partial t} + \rho_0 u\frac{\partial u}{\partial x} + \rho_0 w\frac{\partial u}{\partial y} = -\frac{\partial p}{\partial x} + \mu \Delta u + S_u, \tag{9}$$

$$\rho_0 \frac{\partial w}{\partial t} + \rho_0 u\frac{\partial w}{\partial x} + \rho_0 w\frac{\partial w}{\partial y} = -\frac{\partial p}{\partial y} + \mu \Delta w - g[\rho(T) - \rho_0] + S_w, \tag{10}$$

in which, velocity components, density, thermal conductivity, viscosity and specific heat stand for a linear combination of the proper value for the solid and the liquid phases:

$$u = f_l u_l + (1 - f_l)u_s, \tag{11}$$

$$w = f_l w_l + (1 - f_l)w_s, \tag{12}$$

$$c_p = f_l c_{pl} + (1 - f_l)c_{ps}, \tag{13}$$

$$\kappa = f_l \kappa_l + (1 - f_l)\kappa_s. \tag{14}$$

The source terms at the right hand side of Equations (9) and (10) are responsible for velocity suppression in the solid phase. In our calculation, the following representation of the source terms was applied:

$$S_u = -C\frac{(1 - f_l)^2}{f_l^3 + 0.001}u, \tag{15}$$

$$S_w = -C\frac{(1 - f_l)^2}{f_l^3 + 0.001}w. \tag{16}$$

It describes an implementation of Darcy's law for flow in a porous medium. One may find that, for a temperature grater then T_l, both source terms disappear, and the equations describe pure fluid flow. When local temperature is less than T_s, these terms become dominant ($C = 10^8$), suppressing velocity in the solid phase. In the region where local temperature is between T_s and T_l, flow in the porous medium is simulated (so called "mushy zone").

The thermo-physical properties of ice (the solid phase) were assumed to be constant and equal to their counterparts for water, except for thermal conductivity and density. The value of thermal conductivity for ice $\kappa_s = 2.26\,\text{W/mK}$ and density $\rho = 916.8\,\text{kg/m}^3$ were applied in the codes. The value of latent heat taken was $\lambda = 335\,\text{kJ/kg}$, the temperatures of solidus and liquidus were $T_s = 273.0\,\text{K}$, $T_l = 273.3\,\text{K}$.

The dimensionless parameters defining the problem are the Rayleigh, Prandtl and Stefan numbers: $\text{Ra} = g\beta_0(T_H - T_0)L^3/\alpha\nu = 2\,518\,084$, $\text{Pr} = \nu/\alpha = 6.9$, $\text{Ste} = c_p(T_H - T_0)/\lambda = 0.125$ where $T_0 = 273.0\,\text{K}$ is the melting temperature, and $\beta_0 = 6.734 \cdot 10^{-5}\,1/\text{K}$ is the thermal expansion coefficient at the reference temperature.

3.3. Numerical algorithms and mesh sensitivity test

The problem was solved using the FLUENT 6.0 finite volume code on uniform structural grids (details are given it Table 3). A fully implicit method was used to simulate transient evaluation in time. Time derivatives were approximated using a first

order scheme. Spatial derivatives were approximated using the QUICK scheme, which is based on a weighed average of second-order-upwind and central interpolation of the variable. The pressure-velocity coupling was done using the SIMPLE algorithm. For comparison, the same problem was solved with the NC4MARV2 finite volume code [9], where enthalpy formulation is used for the vorticity-velocity formulation of the Navier-Stokes equations.

Table 3. Discretization meshes used in the calculation

Run No	Mesh name/code	Size	Number of nodes	Number of elements
#8	2d0005/FLUENT	76×76	5 929	5 776
#9	2d0002/FLUENT	190×190	36 481	36 100
#10	2d0001/FLUENT	380×380	145 161	144 400
#11	2d81x81/NC4MARV2	81×81	6 724	6 561

Figure 5 shows profiles of temperature and both velocity components, drawn along the horizontal and vertical symmetry lines of the cavity. The solutions have been obtained for time $t = 100\,$s after freezing has started. Three computational runs (#8, #9, #10 in Table 3) using FLUENT for different meshes are compared. This mesh sensitivity analysis shows that, similarly to the previous case, solutions obtained for the two fine meshes practically overlap. Error for the finest mesh (run #10) is below 1%. The analysis indicates that including the solidification process in FLUENT does not change the mesh sensitivity of the code, at least for the first 100 s of the freezing process. However, the proper modelling requires a very fine mesh and, when combined with the transient solidification process, the simulation becomes very expensive, as there is an additional equation to solve for the new variable – liquid fraction. In the code, liquid fraction is updated during iterations in the way proposed by Rady and Mohanty [12]. This approach introduce an additional internal loop for each time step. Because liquid fraction and temperature are calculated after the velocity components have been obtained, the time step has to be small enough, so that during this time the position of the solid-liquid interface moves less than the diameter of the computational cell. This jeopardises computational time for very fine meshes.

3.4. Analysis of numerical results

Numerical results obtained for water freezing in a differentially heated cavity indicate that in the initial period of time (0–500 s) solidification is much faster than for later time ($> 500\,$s). After 2 600 s, the steady-state seems to have been achieved. During the first 100 s, the thickness of the ice layer is rather uniform, whereas after 100 s the main flow recirculation decreases the solidification rate in the upper part of the cavity and a characteristic belly-like shape of the phase-change front becomes evident (Figure 6).

Numerical results obtained with FLUENT are compared with those obtained with the NC4MARV2 university code. Figure 7 displays profiles of temperature and velocity obtained for both of these codes at the time step $t = 100\,$s. Comparison of the velocity and temperature profiles reveals several discrepancies, especially near the solid-liquid interface. Moreover, there are differences in details of the interface
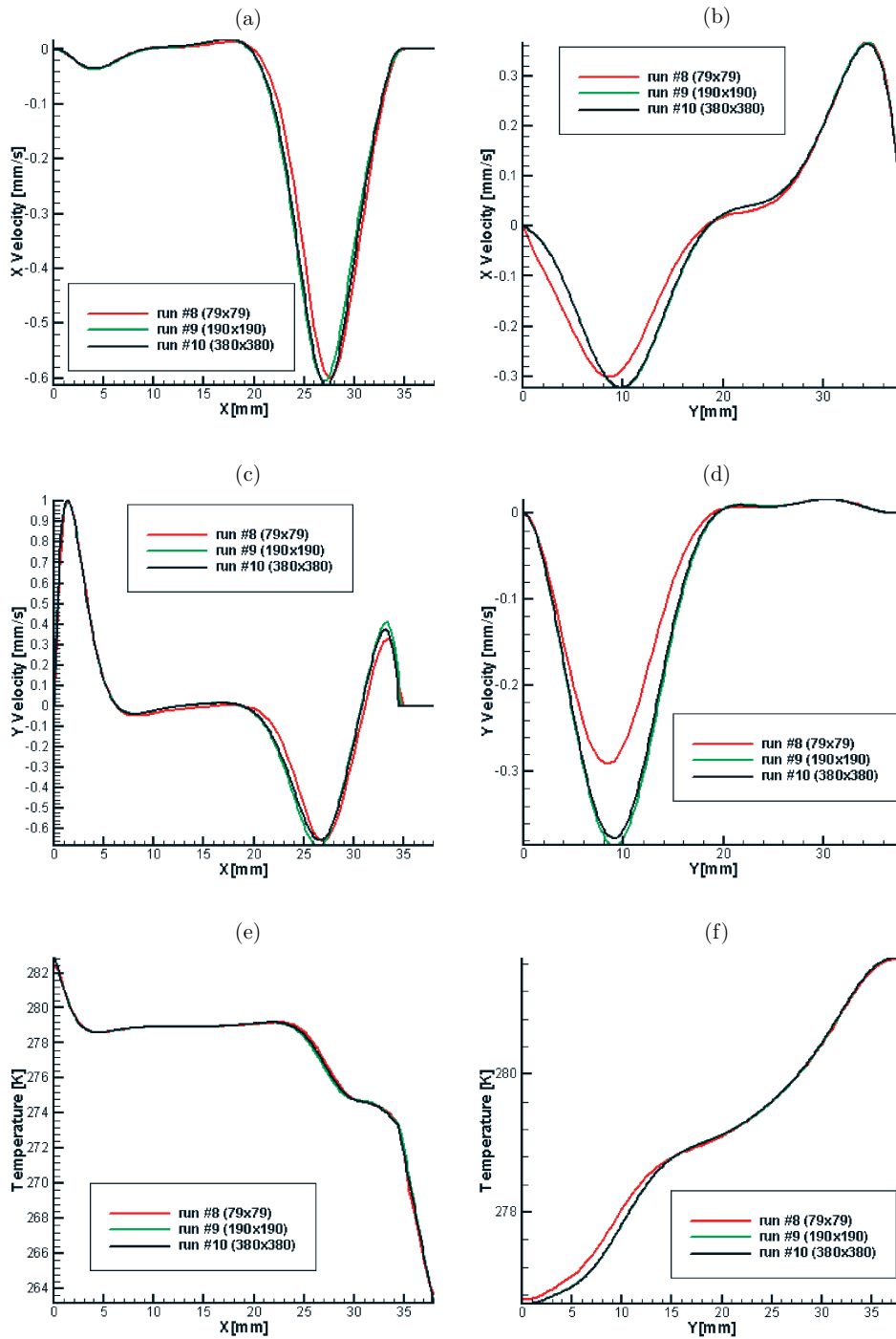
Figure 5. Mesh sensitivity analysis for runs #8, #9, #10, time $t = 100$s. Profiles of the horizontal velocity component (top), the vertical velocity component (middle) and temperature (bottom), taken along the horizontal symmetry line (left column) and along the vertical symmetry line (right column) of the cavity

(a)

(b)

(c)

(d)

(e)

(f)
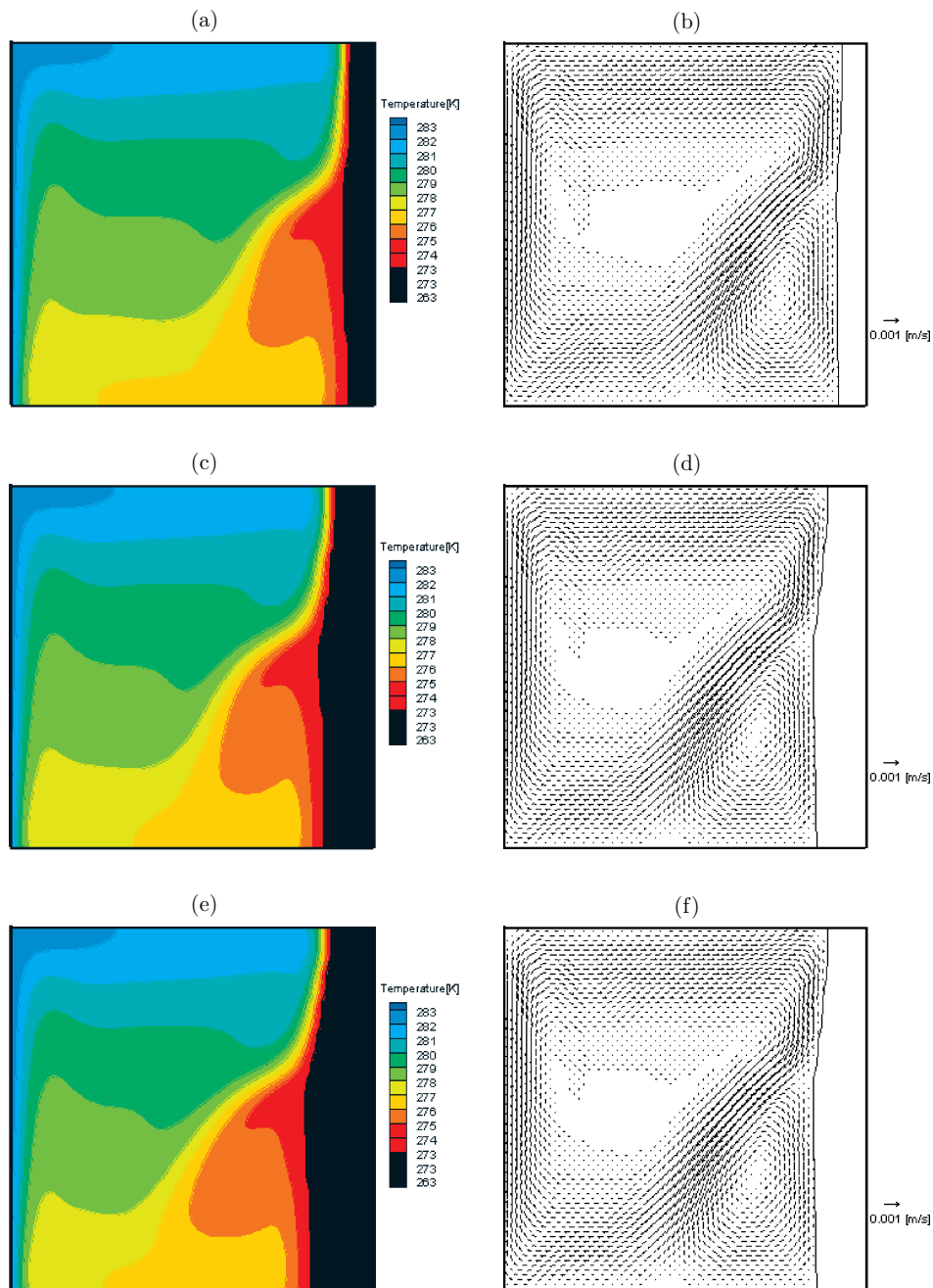
Figure 6. FLUENT solutions (run #8) for freezing water at time steps: 100s – (a), (b);
300s – (c), (d); 500s – (e), (f); temperature contours (left column)
and the velocity vector field (right column); (*continued on the next page*)

profile. The FLUENT solution predicts a rather uniform, flat layer of ice, whereas the
NC4MARV2 code already at that time yields a well-developed "belly" in the middle
part of the ice layer (Figure 8). These differences could arise due to insufficient internal
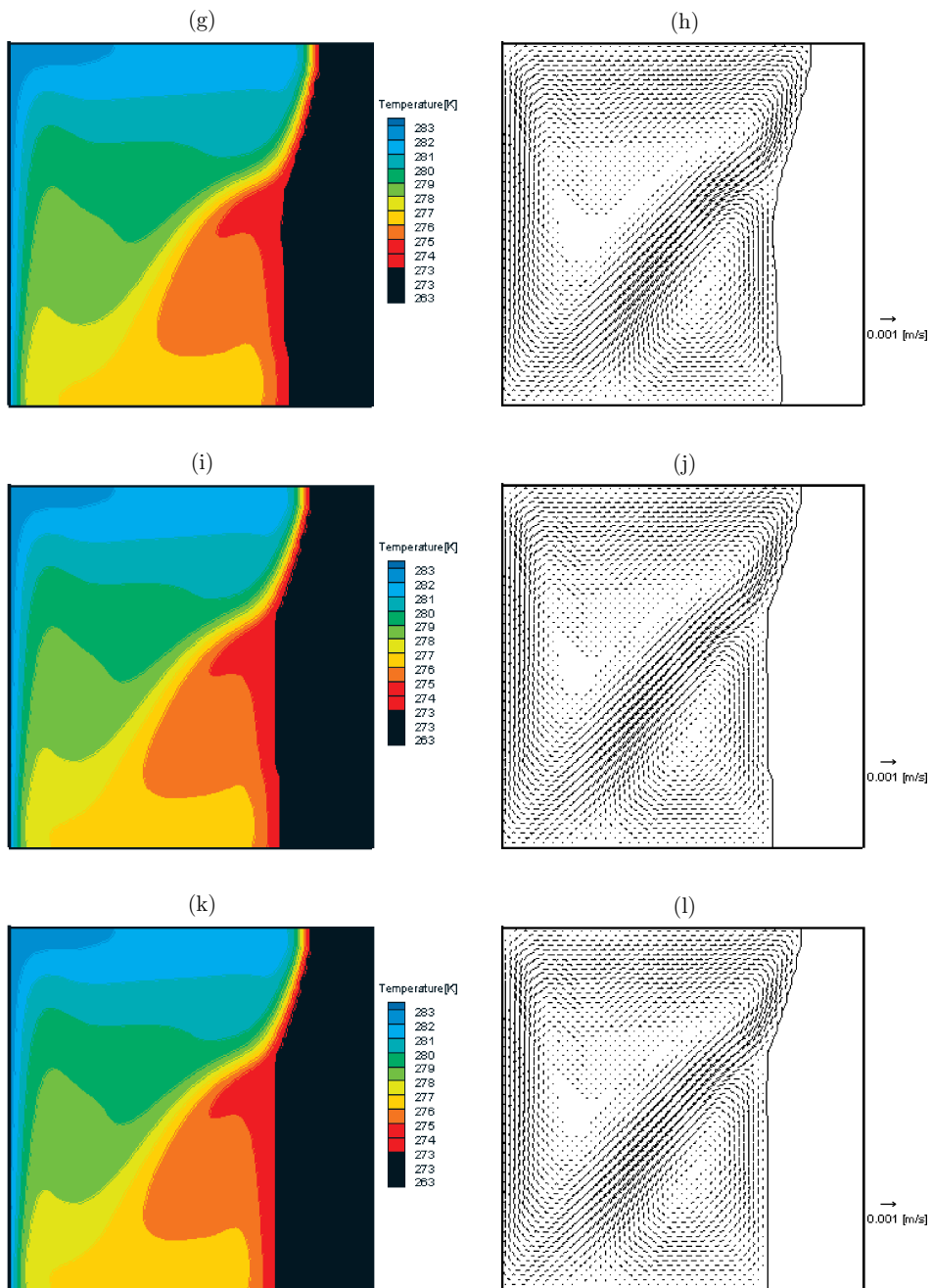
Figure 6 – continued. FLUENT solutions (run #8) for freezing water at time steps: $1\,000\text{s}$ – (g), (h); $2\,000\text{s}$ – (i), (j); $3\,000\text{s}$ – (k), (l); temperature contours (left column) and the velocity vector field (right column)

iterations in solving the energy equations, predefined when using FLUENT. Further numerical analysis is necessary to elucidate this problem. A similar configuration has been studied experimentally by Kowalewski and Rebow [3]. There is relatively good
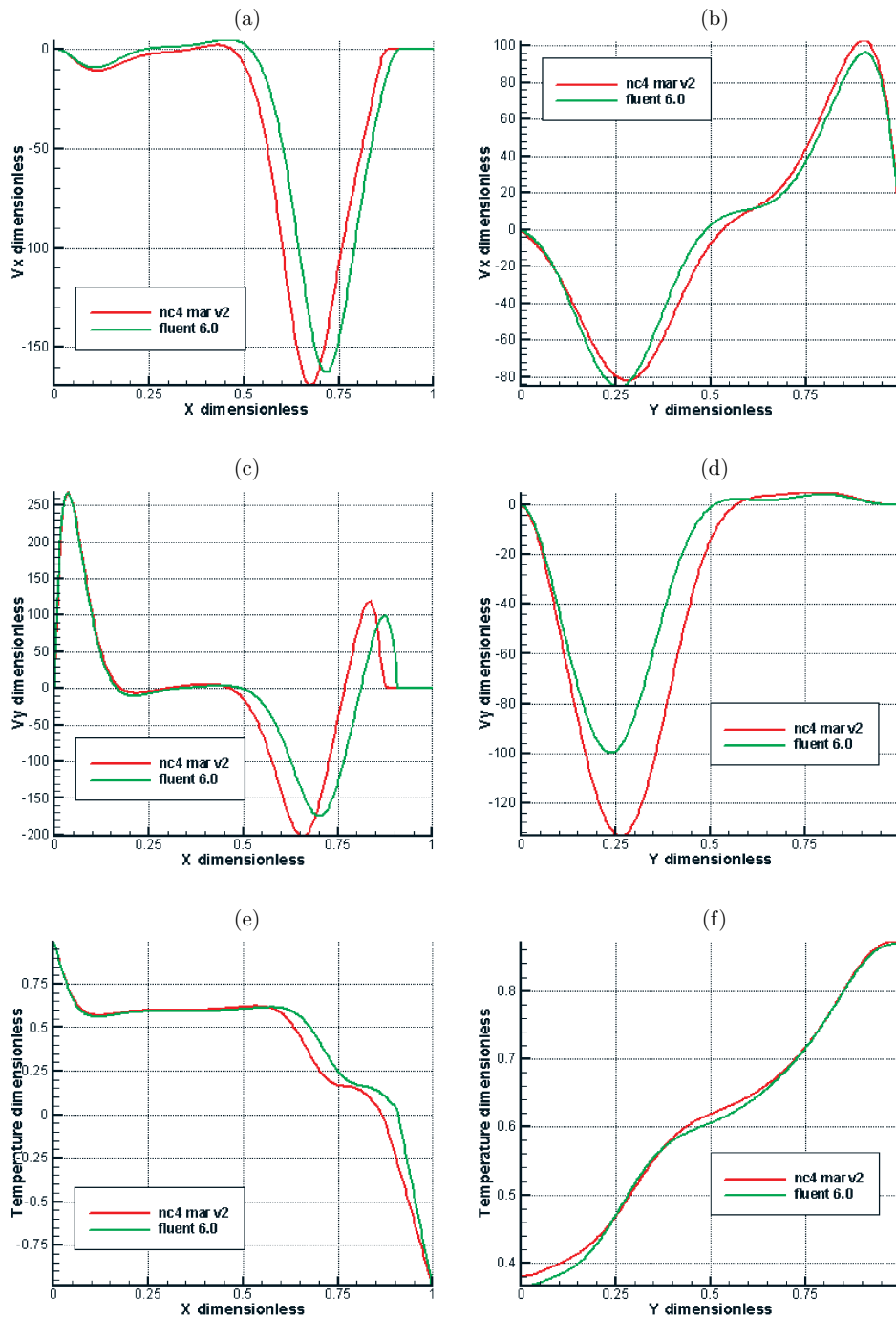
Figure 7. Comparison of the FLUENT solution (run #10) with the NC4MARV2 solution (run #11) at time $t = 100$s. Profiles of the horizontal velocity component (top), the vertical velocity component (middle) and temperature (bottom), taken along the horizontal symmetry line (left column) and along the vertical symmetry line (right column) of the cavity

qualitative agreement for the interface shape and the recirculation pattern. However, a detailed comparison of our simulations with the experimental data is not possible due to differences in the applied boundary conditions and material properties.

(a)   (b)
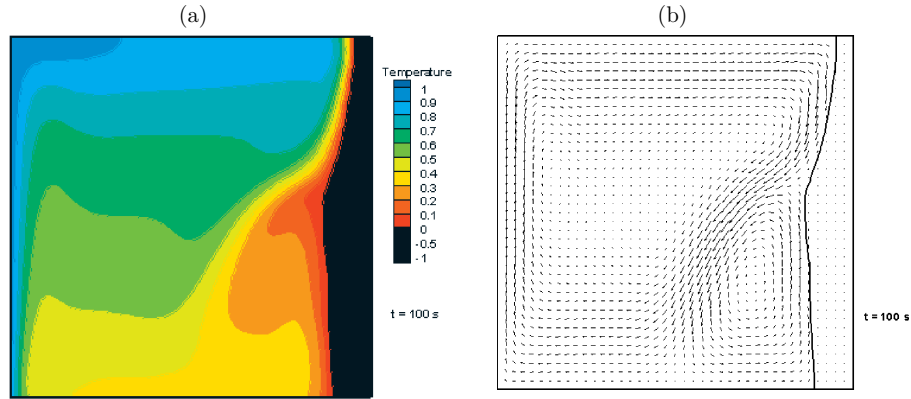
Figure 8. The NC4MARV2 solution (run #11) for freezing water at time step 100s: (a) temperature contours and (b) the velocity vector field

4. Solidification in the presence of free surface flow

4.1. Problem formulation

The third analysed case concerns water freezing during a cavity filling process. The water of initial temperature T_H is forced into an inclined cavity through a circular opening made in the bottom wall. The two opposite walls of the cavity are kept at constant temperatures T_1, T_2 below the freezing point. All other walls of the cavity are assumed to be adiabatic. Both the forced convection and the residual natural convection within the cavity are responsible for heat transfer through the cold side walls. The model attempts to simulate mould filling during a casting process, and it was investigated experimentally by Kowalewski *et al.* [4]. Calculations have been performed to simulate the experimental conditions: the cavity's height is 114 mm and its width is 38 mm (see Figure 9). The inclination angle is $\alpha = 11.4°$. During the filling process, intense mixing of fluid strongly modifies the temperature field, diminishing the solidification rate. As soon as the cavity has been filled up, the inlet is closed and the freezing process dominates. Similar conditions have been applied in the numerical model. Due to the complexity of the problem, involving both solidification and free surface flow, only the two-dimensional case has been solved.
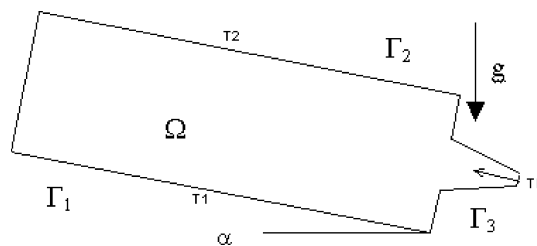
Figure 9. Cross-section of the cavity

4.2. Mathematical formulation

A FLUENT solver using the volume of fluid (VOF) method was used to simulate free surface flow. The freezing of water was modelled using the enthalpy-porosity method, described in the previous section. During the filling process, tracking of the gas-liquid interface is done by solving a continuity equation for volume fraction:

$$\frac{\partial \alpha_1}{\partial t} + u\frac{\partial \alpha_1}{\partial x} + w\frac{\partial \alpha_1}{\partial y} = 0. \tag{17}$$

Volume fraction is an additional variable defined for the gaseous and the fluid phases in such a way that for each computation cell the following condition holds:

$$\alpha_0 + \alpha_1 = 1. \tag{18}$$

Due to the definition of volume fraction, all of the fluid properties included in the conservation equations have the following meaning:

$$\rho = \alpha_0 \rho_0 + \alpha_1 \rho_1, \tag{19}$$

$$\mu = \alpha_0 \mu_0 + \alpha_1 \mu_1, \tag{20}$$

$$c_p = \alpha_0 c_{p0} + \alpha_1 c_{p1}, \tag{21}$$

$$\kappa = \alpha_0 \kappa_0 + \alpha_1 \kappa_1. \tag{22}$$

Thus, during the filling process, the governing equations can be written in the following form:

$$\frac{\partial u}{\partial x} + \frac{\partial w}{\partial y} = 0, \tag{23}$$

$$\rho\frac{\partial u}{\partial t} + \rho u\frac{\partial u}{\partial x} + \rho w\frac{\partial u}{\partial y} = -\frac{\partial p}{\partial x} + \mu\Delta u + S_u + F_\sigma, \tag{24}$$

$$\rho\frac{\partial w}{\partial t} + \rho u\frac{\partial w}{\partial x} + \rho w\frac{\partial w}{\partial y} = -\frac{\partial p}{\partial y} + \mu\Delta w - g\left[\rho(T) - \rho\right] + S_w + F_\sigma, \tag{25}$$

$$\frac{\partial}{\partial t}(\alpha_0\rho_0 c_{p0}T + \alpha_1\rho_1 c_{p1}T) + u\frac{\partial}{\partial x}(\alpha_0\rho_0 c_{p0}T + \alpha_1\rho_1 c_{p1}T) +$$
$$+ w\frac{\partial}{\partial y}(\alpha_0\rho_0 c_{p0}T + \alpha_1\rho_1 c_{p1}T) = \kappa\Delta T - \rho\lambda\frac{\partial f_l}{\partial t}. \tag{26}$$

The interaction between the gas and the liquid phases is incorporated in an additional source term F_σ. The surface force due to the surface tension is interchanged by applying the Gaussian theorem to the volumetric force [13]. This term is defined as a function of surface tension σ, gradient of volume fraction α_1, local curvature of the free surface γ and the average density:

$$F_\sigma = \sigma\frac{\rho\gamma\nabla\alpha_1}{\frac{1}{2}(\rho_0 + \rho_1)}. \tag{27}$$

This term is nil in all computational cells filled by only one phase, due to the gradient of volume fraction. The anomalous thermal variation of water density is implemented only in the buoyancy term in Equation (25), in the same way as in the previous section.

Thermal boundary conditions applied at the two opposite isothermal walls were: $T_1 = 265\,\mathrm{K}$ and $T_2 = 266\,\mathrm{K}$. For other walls other than the inlet, adiabatic boundary

conditions were applied. The temperature of hot water supplied through the inlet was $T_H = 281\,\mathrm{K}$. Standard no-slip boundary conditions were adopted for the velocity components on the walls. At the inlet, a constant velocity $V = 0.0267\,\mathrm{m/s}$ plug flow is assumed. As the initial condition in the empty cavity we assume air at rest at a uniform temperature of $T_o = 298\,\mathrm{K}$. The liquid's temperature at the inlet is constant and equals T_o. The initial volume fraction of the liquid is $\alpha_1 = 0$ in the whole domain. The cavity's height, L (38 mm), is used to scale non-dimensional variables. These conditions correspond to the experimental data.

Thermophysical values specific for each phase used in the calculations are collected in Table 4. These values are based on the default database included in the FLUENT code.

Table 4. Properties of the water and air used in the calculations

Material properties of air and water	Value	Unit
ρ_1 density of air at reference temperature $T = 288\,\mathrm{K}$	1.225	kg/m^3
μ_1 dynamic viscosity of air (at $T = 288\,\mathrm{K}$)	$1.7894 \cdot 10^{-5}$	kg/ms
κ_1 thermal conductivity of air (at $T = 288\,\mathrm{K}$)	0.0242	W/mK
c_{p1} specific heat of air (at $T = 288\,\mathrm{K}$)	1006.43	J/kgK
ρ_0 density of water at reference temperature ($T = 273\,\mathrm{K}$)	999.8	kg/m^3
μ_0 dynamic viscosity of water ($T = 288\,\mathrm{K}$)	0.001003	kg/ms
$\nu_0 = \mu_0/\rho_0$ kinematic viscosity (at $T = 288\,\mathrm{K}$)	$1.0032 \cdot 10^{-6}$	m^2/s
κ_0 thermal conductivity of water ($T = 288\,\mathrm{K}$)	0.6	W/mK
c_{p0} specific heat of water ($T = 288\,\mathrm{K}$)	4182.0	J/kgK
β_0 thermal expansion coefficient (at $T = 273\,\mathrm{K}$)	$6.734 \cdot 10^{-5}$	1/K
σ surface tension	0.0735	N/m
λ latent heat	335	kJ

The dimensionless parameters defining the problem are the Rayleigh, Prandtl, Stefan and Reynolds numbers: $\mathrm{Ra} = g\rho_0 c_{p0}\beta_0(T_H - T_0)L^3/\kappa_0\nu_0 = 1\,762\,582$, $\mathrm{Pr} = \nu_0\rho_0 c_{p0}/\kappa_0 = 6.99$, $\mathrm{Ste} = c_{p0}(T_H - T_0)/\lambda = 0.0999$, $\mathrm{Re} = \rho_0 v_{inlet}L/\mu_0 = 100 - 500$.

4.3. Discretization and numerical algorithm

The cavity filling problem was solved using four different uniform structural grids (Table 5). A fully implicit method was used to simulate transient evaluation in time. The time derivative was approximated using a first order scheme. Spatial derivatives were approximated using a first order upwind scheme. The pressure-velocity coupling was done using the PISO algorithm with skewness correction at each time step.

The mesh sensitivity analysis shows quite serious differences in the obtained solutions, persistent even for the finest meshes. Differences are especially apparent near the free surface. It seems necessary to apply local mesh refinement at the interface to stabilise the solution during transient modifications of the interface.

Table 5. Discretization meshes used in the calculation

Run No	Mesh name/code	Size	Number of nodes	Number of elements
#12	2d001/FLUENT	38×114	4800	4626
#13	2d0005/FLUENT	76×228	18822	18476
#14	2d0002/FLUENT	190×570	116374	115510
#15	2d0001/FLUENT	380×1140	463767	462040
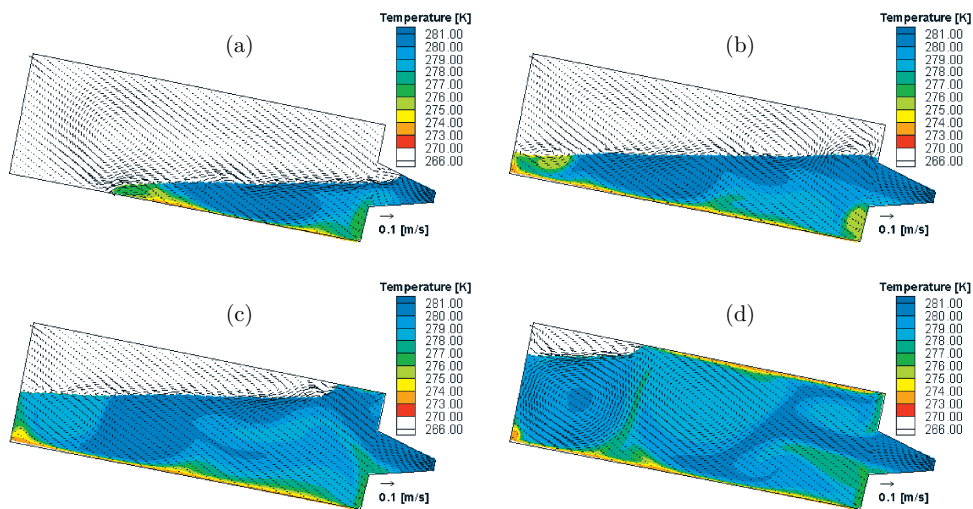
Figure 10. Temperature and velocity fields during the free surface flow phase (run #13) at:
(a) $t = 10$s, (b) $t = 20$s, (c) $t = 30$s, (d) $t = 40$s
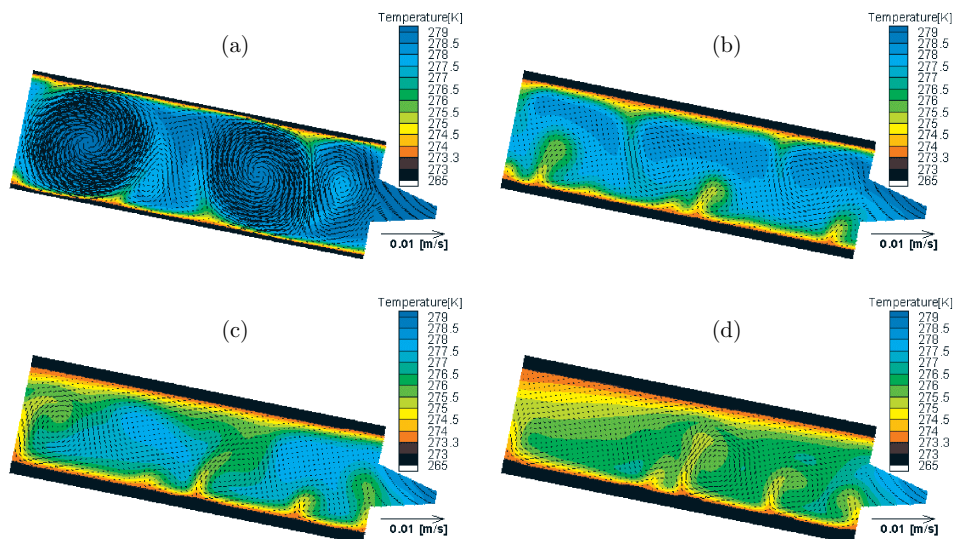
Figure 11. Temperature and velocity fields during the freezing phase (run #13) at:
(a) $t = 73$s; (b) $t = 173$s; (c) $t = 273$s, (d) $t = 373$s

4.4. Analysis of preliminary results

Preliminary numerical results of temperature and velocity field obtained for a relatively coarse mesh (run #13) are given in Figures 10 and 11. Initially, during the filling process, the simulation indicates the presence of several counter-rotating circulation patterns. A similar pattern was observed in the experiments [4]. Initially, the hot fluid penetrated the cavity mainly along the free surface, creating a thermally stratified configuration. When more than half of the cavity was filled, a characteristic recirculation pattern appeared. After the valve was closed, the fluid trapped in the cavity started to cool. The thermal conductivity of the fluid supported by natural convection attempted to homogenise temperature distribution in the cavity. Our simulation shows relatively uniform growth of the ice layer, both for the upper and the lower walls.

There are serious discrepancies between the simulated and the experimental results. The most distinct difference is the lack of the ice layer in the numerical simulations during the first filling phase. One of the most probable sources of these differences is inaccurate information obtained from the experiment for the thermal boundary conditions at two metal walls. Our assumption of the isothermal conditions seems to be wrong, and detailed experimental data about temperature variation at the side walls must be implemented in the code. However, in spite of these differences, the main flow patterns obtained for the second phase of the process are qualitatively in agreement with the experimental data.

5. Conclusions

The FLUENT commercial code was used to simulate convection of water associated with the freezing process. Three numerical solutions are presented. The steady-state solution for natural convection of water close to the freezing point has been positively verified using the FRECON3V university code [8]. This solution can be proposed as a benchmark for comparing and verifying numerical codes. The second solution, obtained using the fixed grid enthalpy-porosity method, shows only qualitative agreement with the reference solution [9]. Further investigations are necessary to select a correct solution for this configuration. The third solution concerns a complex flow configuration, combining free surface flow, forced convection and solidification. Our preliminary numerical investigation indicates problems with modelling free surface flow. An additional re-meshing procedure seems to be necessary to accurately follow the progressing fluid surface.

It appears that modelling the freezing of water requires very fine meshes and small time steps. Using refined meshes cause a tremendous decrease of code performance, hardly acceptable for simulation of practical and technological processes. Further studies are necessary to overcome this problem.

Acknowledgements

References

[1] Ramachandran N, Gupta J P and Jaluria Y 1982 *Int. J. Heat Mass Transfer* **25** 187

[2] Viswanath R and Jaluria Y 1993 *Num. Heat Transfer, Part B* **24** 77

[3] Kowalewski T A and Rebow M 1999 *Int. J. Comp. Fluid Dyn.* **11** 193

[4] Kowalewski T A, Cybulski A and Michałek T 2002 *Heat Transfer* **4** 813

[5] 2002 *FLUENT 6.0, Users Guide*, Fluent Inc., Lebanon, NH

[6] Giangi M, Stella F and Kowalewski T A 1999 *Comput. Visual. Sci.* **2** 123

[7] Voller V R, Cross M and Markatos N C 1987 *Int. J. Num. Meth. in Eng.* **24** 271

[8] Leonardi E, Kowalewski T A, Timchenko V and de Vahl Davis G 1999 *Proc. Int. Conf. Comp. Heat and Mass Transfer* (Mohamad A A and Sezai I, Eds.), Cyprus, Eastern Mediterranean University Printinghouse, pp. 182–188

[9] Giangi M, Kowalewski T A, Stella F and Leonardi E 2000 *Computer Assisted Mechanics and Engineering Scinces* **7** 321

[10] De Vahl Davis G 1983 *Int. J. Num. Meth. in Fluids* **3** 249

[11] Patankar S V 1980 *Numerical Heat Transfer and Fluid Flow*, Hemisphere, Washington, D.C.

[12] Rady M A and Mohanty A K 1996 *Num. Heat Transfer, Part A* **29** 49

[13] Brackbill J U, Kothe D B and Zemach C 1992 *J. Comp. Phys.* **100** 335